

Induced Polarization in the $^2\text{H}(\gamma, \vec{n})^1\text{H}$ Reaction at Low Energy

R. Schiavilla

Jefferson Lab, Newport News, Virginia 23606
 Department of Physics, Old Dominion University,
 Norfolk, Virginia 23529

(Dated: July 29, 2018)

The induced polarization, P'_y , of the neutron in the deuteron photo-disintegration from threshold up to 30 MeV is calculated using a variety of different, latest-generation potentials—Argonne v_{18} , Bonn 2000, and Nijmegen I—and a realistic model for the nuclear electromagnetic current operator, including one- and two-body terms. The model dependence of the theoretical predictions is found to be very small. These predictions are systematically larger in magnitude than the measured P'_y values, and corroborate the conclusions of an earlier, and much older, study. There is considerable scatter in the available experimental data. New and more accurate measurements of the induced polarization in the $^2\text{H}(\gamma, \vec{n})^1\text{H}$ reaction are needed in order to establish unequivocally whether there is a discrepancy between theory and experiment.

PACS numbers: 21.30.+y, 25.20.Lj, 24.70.+s, 25.10.+s

I. INTRODUCTION, RESULTS, AND CONCLUSIONS

The present note deals with the deuteron photo-disintegration and neutron induced polarization in the $^2\text{H}(\gamma, \vec{n})^1\text{H}$ reaction at low energy, from threshold up to about 30 MeV. In this energy range, the photo-disintegration process is dominated by the contributions of electric dipole ($E1$) and, to a much less but still significant extent, electric quadrupole ($E2$) transitions, connecting the deuteron to the np $^3\text{P}_{J=0,1,2}$ and $^3\text{S}_1$ – $^3\text{D}_1$ states, respectively. The experimental data are well reproduced by theory, see Refs. [1, 2] and Figs. 1–3. The total cross section data are from Refs. [3, 4, 5, 6, 7, 8, 9, 10, 11], the angular distribution data at photon energy $E_\gamma=19.8$ MeV are from Ref. [12], and the data on angular distribution ratios as function of E_γ are from Ref. [13]. The calculations shown in these figures, various aspects of which are succinctly summarized in the following section, are based on a variety of (modern) realistic nucleon-nucleon potentials, including the CD-Bonn (BONN) [14], Nijmegen I (NIJM-I) [15], and Argonne v_{18} (AV18) [16], as well as on semi-realistic reductions of the AV18 [17], the Argonne v_6 (AV6) and Argonne v_8 (AV8) models, constrained to reproduce the binding energy of the deuteron and the isoscalar combination of the S- and P-wave phase shifts. In particular, the AV6 ignores spin-orbit interaction components, which are important in differentiating among the $^3\text{P}_{0,1,2}$ channels, and therefore does not provide a good fit to the phase shifts in these channels. The model dependence of all theoretical predictions shown in Figs. 1–3, including those corresponding to the AV6 and AV8 in Fig. 1, is negligible.

Calculations of the np radiative capture cross section at thermal neutron energies, based on these same potential models, are also found to be in excellent agreement with the measured value, when two-body current contributions are taken into account [1, 2]. The model dependence is again negligible. The np radiative capture up to neutron energies of about 100 keV proceeds almost exclusively through the well-known magnetic dipole ($M1$) transition connecting the $^1\text{S}_0$ np and deuteron states [18].

On the basis of these facts, one is led to conclude that the $M1$ and $E1$ transition strengths, which the np radiative capture and deuteron photo-disintegration are selectively sensitive to at low energies, are both consistent with experimental data. It is known [19] that the neutron induced polarization (P'_y) in the $^2\text{H}(\gamma, \vec{n})^1\text{H}$ reaction originates predominantly, in the low-energy regime of interest here, from interference of $M1$ and $E1$ transition terms. Thus, it is surprising to find that this observable, measured up to photon energies of 25 MeV, is significantly overestimated, in magnitude, by theory, as shown in Figs. 4–6, although the data at the (center-of-mass) angle of 135° in Fig. 7 seem to be consistent with it. The P'_y angular distribution data at $E_\gamma=2.75$ MeV are from Refs. [20, 21, 22], while the data at $\theta=90^\circ$ for $E_\gamma=6$ –30 MeV are from Refs. [23, 24, 25], and those at $\theta=45^\circ$ and 135° are from Refs. [23] and [25, 26], respectively. In the figures the results obtained without (IA) and with the inclusion of two-body current contributions are displayed separately for the BONN, NIJM-I, and AV18 potential models. The contributions of two-body currents, essential if the observed cross section for the np radiative capture is to be correctly predicted, turn out to substantially worsen the agreement between the measured and calculated P'_y in all cases but at $\theta=135^\circ$. The discrepancy between theory and experiment is particularly severe for P'_y at $\theta=45^\circ$.

That the P'_y data are problematic for theory has in fact been known for some time [25, 26, 27, 28]. Indeed, the main motivation for the present study was to re-examine this issue in light of the advances made during the last decade in the modeling of both nucleon-nucleon potentials and two-body electromagnetic currents. The corresponding results, however, are close to those of Hadjimichael [27]—reported in Ref. [25] at $\theta=90^\circ$ —and Schmitt *et al.* [28] and, moreover,

show a very small model dependence. There is considerable scatter among the different data sets at $\theta=90^\circ$ and in the measurements of the P'_y angular distribution at $E_\gamma=2.75$ MeV. Clearly, more accurate data on both the energy dependence and angular distribution, which could be used to isolate the multipole components, are needed in order to resolve this confusing situation, and draw definite conclusions.

II. CALCULATION

The relevant matrix element in the photo-disintegration of a deuteron in spin projection m_d initially at rest in the laboratory is

$$j_{m_n, m_p; \lambda, m_d}^{(-)}(\mathbf{p}, \mathbf{q}) = \langle \mathbf{q}; \mathbf{p}, m_n, m_p | \hat{\epsilon}_\lambda(\mathbf{q}) \cdot \mathbf{j}(\mathbf{q}) | m_d \rangle \quad (2.1)$$

where \mathbf{q} is the momentum of the absorbed photon and $\hat{\epsilon}_\lambda, \lambda = \pm 1$, are the spherical components of its polarization vector, $\mathbf{j}(\mathbf{q})$ is the nuclear electromagnetic current operator, and $|\mathbf{q}; \mathbf{p}, m_n, m_p\rangle^{(-)}$ represents an np scattering state with total momentum \mathbf{q} and relative momentum \mathbf{p} , satisfying incoming wave boundary conditions. The z -axis is taken along $\hat{\mathbf{q}}$, which also defines the spin-quantization axis. In the results of the calculations presented in Sec. I, the np state includes all channels up to total angular momentum $J=5$, the contributions of higher partial waves have been found numerically negligible. The methods used to solve for the two-nucleon bound- and scattering-state problems as well as the techniques developed for the evaluation of the transition amplitudes above have been described in considerable detail in Ref. [1]: they will not be discussed further here.

It is convenient to introduce a second reference frame with axes \mathbf{x}' , \mathbf{y}' , and \mathbf{z}' , in which the relative momentum \mathbf{p} is along \mathbf{z}' with components $(\sin\theta \cos\phi, \sin\theta \sin\phi, \cos\theta)$ with respect to the reference frame defined earlier. The \mathbf{x}' and \mathbf{y}' axes are taken to have directions $(\cos\theta \cos\phi, \cos\theta \sin\phi, -\sin\theta)$ and $(-\sin\phi, \cos\phi, 0)$, respectively. A neutron with polarization in the $+\mathbf{y}'$ direction, as an example, is represented by the state

$$|+\mathbf{y}'\rangle = \frac{|+\rangle + i e^{i\phi} |-\rangle}{\sqrt{2}}, \quad (2.2)$$

where $|\pm\rangle$ denote the spin states with $\pm 1/2$ projections along $\hat{\mathbf{z}}$, i.e. $\hat{\mathbf{q}}$. The transition amplitude for emission of a neutron with polarization in the $+\mathbf{y}'$ direction is then obtained from the linear combination

$$j_{+\mathbf{y}', m_p; \lambda, m_d}^{(-)} = \frac{1}{\sqrt{2}} \left[j_{+, m_p; \lambda, m_d}^{(-)} - i e^{-i\phi} j_{-, m_p; \lambda, m_d}^{(-)} \right]. \quad (2.3)$$

A similar expression holds for emission of a neutron with polarization in the $-\mathbf{y}'$ direction. The induced polarization P'_y is defined as

$$P'_y = \frac{\sigma_{+\mathbf{y}'}(\theta) - \sigma_{-\mathbf{y}'}(\theta)}{\sigma_{+\mathbf{y}'}(\theta) + \sigma_{-\mathbf{y}'}(\theta)}, \quad (2.4)$$

where the differential cross section is given by

$$\sigma_{\pm \mathbf{y}'}(\theta) \equiv \frac{d\sigma_{\pm \mathbf{y}'}}{d\Omega} = \frac{\alpha}{24\pi} \frac{m p}{q} \sum_{m_d, \lambda} \sum_{m_p} |j_{\pm \mathbf{y}', m_p; \lambda, m_d}^{(-)}(\mathbf{p}, \mathbf{q})|^2. \quad (2.5)$$

Here α is the fine structure constant, m is the nucleon mass, and the magnitude p of the relative momentum is fixed by energy conservation. The polarization parameters P'_x and P'_z , proportional to cross-section differences for emission of neutrons with polarizations, respectively, in the $\pm \hat{\mathbf{x}'}$ and $\pm \hat{\mathbf{z}'}$ directions, vanish, as required by parity conservation, and this fact has been explicitly verified in the numerical calculations.

The continuity equation allows one to express the nuclear electromagnetic current entering Eq. (2.1) as [1]

$$\mathbf{j}(\mathbf{q}) = \mathbf{j}(\mathbf{q}) - \mathbf{j}(\mathbf{q}=0) + i \left[H, \int d\mathbf{x} \mathbf{x} \rho(\mathbf{x}) \right], \quad (2.6)$$

where H is nuclear Hamiltonian and $\rho(\mathbf{x})$ is the nuclear charge density operator. This identity ensures that the Siegert form is used for the $E1$ operator, dominant in the energy regime of interest here. Note that the matrix elements $j_{+y',m_p;\lambda,m_d}^{(-)}$ are calculated as discussed in Ref. [1], namely without performing the expansion of $\mathbf{j}(\mathbf{q})$ in terms of electric and magnetic multipole operators. Of course, the commutator term in Eq. (2.1) reduces to

$$i \int d\mathbf{x} \mathbf{x} [H, \rho(\mathbf{x})] \rightarrow iq \int d\mathbf{x} \mathbf{x} \rho(\mathbf{x}) \equiv iq \mathbf{d} , \quad (2.7)$$

when evaluating the matrix elements. The dominant contribution \mathbf{d}^{NR} to the electric dipole operator \mathbf{d} , to which the (unretarded) $E1$ multipole operator is proportional, is simply given by

$$\mathbf{d}^{\text{NR}} = \sum_i P_i(\mathbf{r}_i - \mathbf{R}) , \quad (2.8)$$

where $\mathbf{R} = (\mathbf{r}_1 + \mathbf{r}_2)/2$ is the center-of-mass position vector and P_i is the proton projector. However, there are a number of relativistic corrections which have been included in the present study, due to i) the spin-orbit term in the single-nucleon charge density operator, ii) the leading two-body contribution to $\rho(\mathbf{x})$, associated with pion exchange, and iii) the center-of-energy correction. Explicit expressions for the associated operators can be found in Refs. [29, 30]. In particular, the center-of-energy correction arises because translationally invariant wave functions require center-of-energy rather than center-of-mass coordinates. The correct electric dipole operator should be defined as

$$\mathbf{d} = \sum_i P_i(\mathbf{r}_i - \mathbf{R}_{\text{CE}}) , \quad (2.9)$$

where

$$\mathbf{R}_{\text{CE}} = \frac{1}{2} \left(\frac{1}{\sum_i E_i} \sum_i E_i \mathbf{r}_i + \text{h.c.} \right) , \quad (2.10)$$

and (for two particles)

$$E_i \simeq m + \frac{\mathbf{p}_i^2}{2m} + \frac{v_{12}}{2} . \quad (2.11)$$

This leads to a correction term to \mathbf{d}^{NR} of the form

$$\mathbf{d}^{\text{CE}} = \mathbf{R} - \mathbf{R}_{\text{CE}} \simeq -\frac{1}{8m^2} \left[\frac{1}{1 + H/(2m)} (\mathbf{p} \cdot \mathbf{P}) \mathbf{r} + \text{h.c.} \right] , \quad (2.12)$$

for transitions between states with zero z -component of the total isospin, \mathbf{P} is the pair total momentum. Quantitatively, however, this as well as the spin-orbit and pion-exchange corrections to \mathbf{d}^{NR} have been found to be rather small for E_γ up to 30 MeV (see below). It is interesting to note that in the ${}^4\text{He}(d, \gamma){}^6\text{Li}$ radiative capture, the matrix elements of \mathbf{d}^{NR} vanish because of isospin selection rules (and the use of translationally invariant wave functions), and the relativistic corrections above are responsible for the $E1$ strength which dominates the cross section for this process at energies of 100 keV and below [30].

The two-body currents in the calculations based on the BONN and NIJM-I potentials include the terms associated with π - and ρ -meson exchanges, Δ -excitation, and $\rho\pi\gamma$ and $\omega\pi\gamma$ transition mechanisms (see Ref. [1] and references therein). The AV18 calculation includes, in addition, the two-body currents associated with its momentum-dependent interaction components, as derived in Ref. [2]. It should be emphasized that the AV18 currents are exactly conserved.

Finally, Fig. 8 is meant to illustrate the sensitivity of the P'_g results to various inputs in the calculation. The curves labeled AV18, AV8 and AV6 denote the results of calculations based on the AV18, AV8 and AV6 potentials, respectively, including one- and two-body currents [2] and the relativistic corrections to the electric dipole operator discussed above (the curves labeled BONN, NIJM-I and AV18 in Figs. 1–7 are obtained in this same approximation scheme, while those labeled BONN IA, NIJM-I IA, and AV18 IA ignore two-body current contributions). As already

emphasized, this polarization observable is not very sensitive to the input potential, even in the case of a semi-realistic one like the AV6. The curves labeled AV18 IA and AV18 IA w/o RC in E1 both represent AV18-based results including only one-body currents, the difference being that in the AV18 IA w/o RC in E1 calculation the relativistic corrections to \mathbf{d}_{NR} are ignored, while in the AV18 IA one they are retained. At the highest energy, the associated contributions reduce (in magnitude) the AV18 IA results by about 5% (in the total cross section they decrease the AV18 IA values by less than 1% over the whole E_{γ} range). The curve labeled AV18 S+P shows the AV18-based results obtained by including one- and two-body currents, but only S- and P-waves in the partial-wave expansion of the final np state. As can be seen by comparing the AV18 and AV18 S+P curves, the contributions of the higher partial waves to P'_y are substantial at the highest photon energies. Lastly, the results denoted as AV18 w/o M1 are obtained with the AV18, except that the contribution of the $M1$ transition due to the 1S_0 state has been neglected. It demonstrates the sensitivity of the P'_y observable at $\theta=90^\circ$ to this component of the amplitude [19]. This sensitivity persists at $\theta=45^\circ$ and 135° . Note that the total cross section in Fig. 1 is reduced by less than 1% for E_{γ} in the 4-6 MeV range.

Acknowledgments

The author wishes to thank Roy Holt for stimulating his interest in the ${}^2\text{H}(\gamma, \vec{n}){}^1\text{H}$ reaction, Ron Gilman and Roy Holt for a critical reading of the manuscript, Gerry Hale and Ron Gilman for making available to him experimental data sets of the deuteron photo-disintegration cross section and neutron induced polarization observable, respectively. The author's work was supported by DOE contract DE-AC05-84ER40150 under which the Southeastern Universities Research Association (SURRA) operates the Thomas Jefferson National Accelerator Facility. Finally, the calculations were made possible by grants of computing time from the National Energy Research Supercomputer Center.

[1] R. Schiavilla, J. Carlson, and M. Paris, Phys. Rev. C **70**, 044007 (2004).
 [2] L.E. Marcucci, M. Viviani, R. Schiavilla, A. Kievsky, and S. Rosati, nucl-th/0502048 and Phys. Rev. C in press.
 [3] G.R. Bishop *et al.*, Phys. Rev. **80**, 211 (1950).
 [4] A.H. Snell, E.C. Barker, and R.L. Sternberg, Phys. Rev. **80**, 637 (1950).
 [5] S.A. Colgate, Phys. Rev. **83**, 1262 (1951).
 [6] J.H. Carver *et al.*, Nature **167**, 154 (1951).
 [7] J. Ahrens *et al.*, Phys. Lett. **52B**, 49 (1974).
 [8] Y. Birenbaum, S. Kahane, and R. Moreh, Phys. Rev. C **32**, 1825 (1985).
 [9] R. Bernabeu *et al.*, Phys. Rev. Lett. **57**, 1542 (1986).
 [10] R. Moreh, T.J. Kennett, and W.V. Prestwich, Phys. Rev. C **39**, 1247 (1989).
 [11] A. De Graeve *et al.*, Phys. Rev. C **45**, 860 (1992).
 [12] M.P. De Pascale *et al.*, Phys. Rev. C **32**, 1830 (1985).
 [13] K.E. Stephenson, R.J. Holt, R.D. McKeown, and J.R. Specht, Phys. Rev. C **35**, 2023 (1987).
 [14] R. Machleidt, Phys. Rev. C **63**, 024001 (2001).
 [15] V.G.J. Stoks, R.A.M. Klomp, C.P.F. Terheggen, and J.J. de Swart, Phys. Rev. C **49**, 2950 (1994).
 [16] R.B. Wiringa, V.G.J. Stoks, and R. Schiavilla, Phys. Rev. C **51**, 38 (1995).
 [17] R.B. Wiringa and S.C. Pieper, Phys. Rev. Lett. **89**, 182501 (2002).
 [18] L.E. Marcucci, K.M. Nollett, R. Schiavilla, and R.B. Wiringa, nucl-th/0402078 and Nucl. Phys. A in press.
 [19] M.L. Rustgi, W. Zernik, G. Breit, and D.J. Andrews, Phys. Rev. **120**, 1881 (1960).
 [20] W. John and F.V. Martin, Phys. Rev. **124**, 830 (1961).
 [21] R. Bösch, J. Lang, R. Müller, and W. Wölfli, Helv. Phys. Acta **36**, 657 (1963).
 [22] R.W. Jewell, W. John, J.E. Sherwood, and D.H. White, Phys. Rev. **139**, B71 (1965).
 [23] R. Nath, F.W.K. Firk, and H.L. Schultz, Nucl. Phys. A **194**, 49 (1972).
 [24] L.J. Droucks, Ph.D. thesis, Yale University, 1976 (unpublished).
 [25] R.J. Holt, K. Stephenson, and J.R. Specht, Phys. Rev. Lett. **50**, 577 (1983).
 [26] R.J. Holt, private communication.
 [27] E. Hadjimichael, Phys. Lett. **46B**, 147 (1973).
 [28] K.-M. Schmitt, P. Wilhelm, and H. Arenhövel, Few-Body Syst. **10**, 105 (1991).
 [29] M. Viviani, A. Kievsky, L.E. Marcucci, S. Rosati, and R. Schiavilla, Phys. Rev. C **61**, 064001 (2000).
 [30] K.M. Nollett, R.B. Wiringa, and R. Schiavilla, Phys. Rev. C **63**, 024003 (2001).

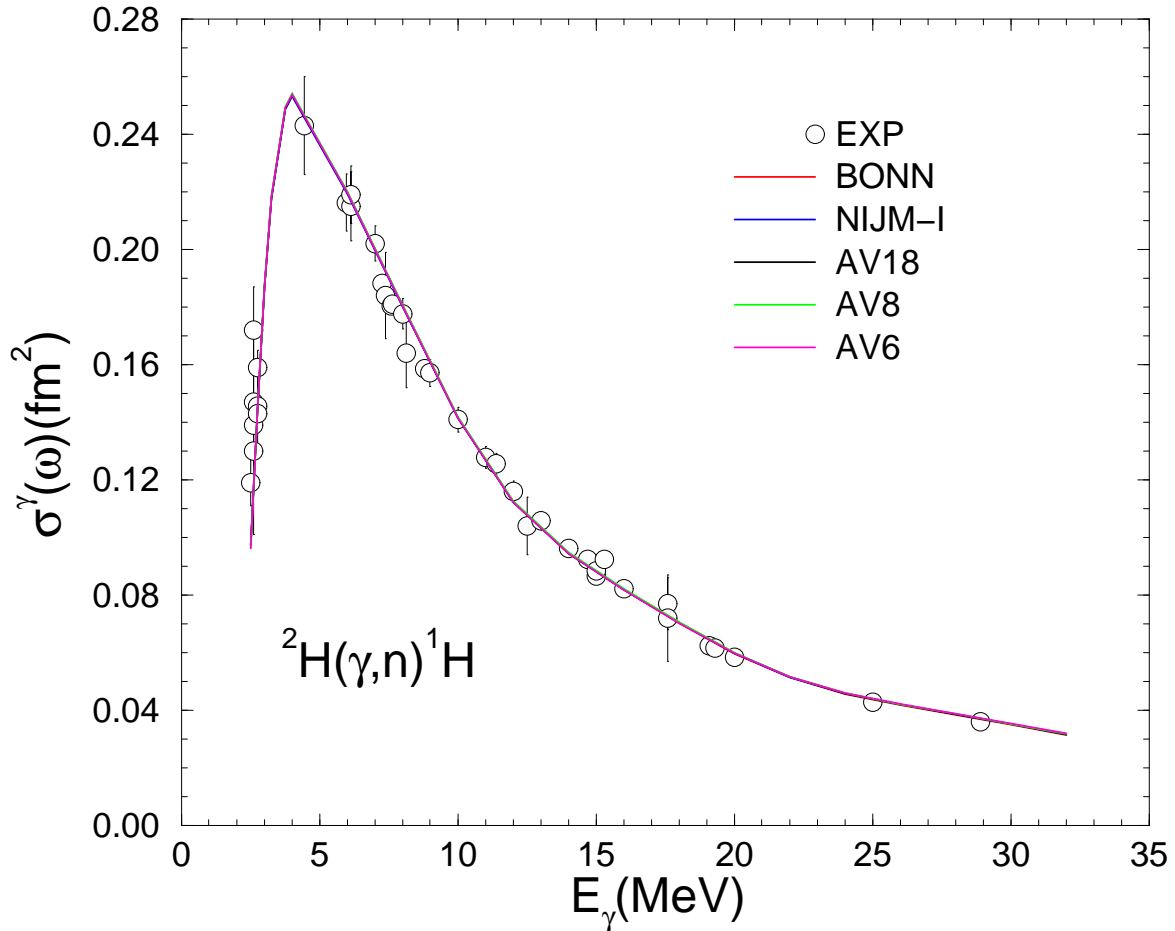


FIG. 1: (Color online) The deuteron photo-disintegration cross section, calculated with a number of modern nucleon-nucleon potentials, is compared to data. Note that the various curves are indistinguishable.

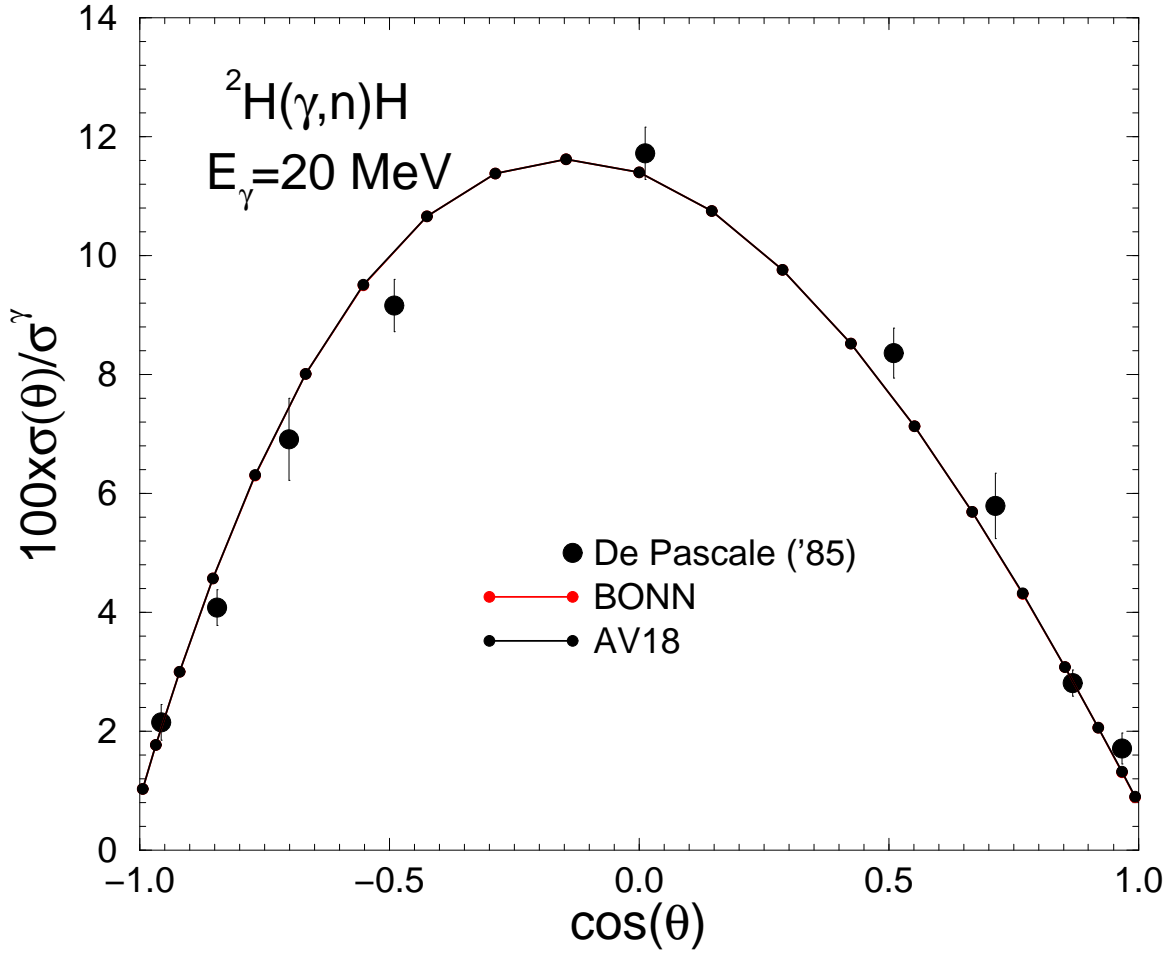


FIG. 2: (Color online) The center-of-mass angular distribution of the experimental photo-disintegration cross section, normalized to the total cross section, is compared to the results of calculations based on the BONN and AV18 potentials. Note that the theoretical curves are indistinguishable.

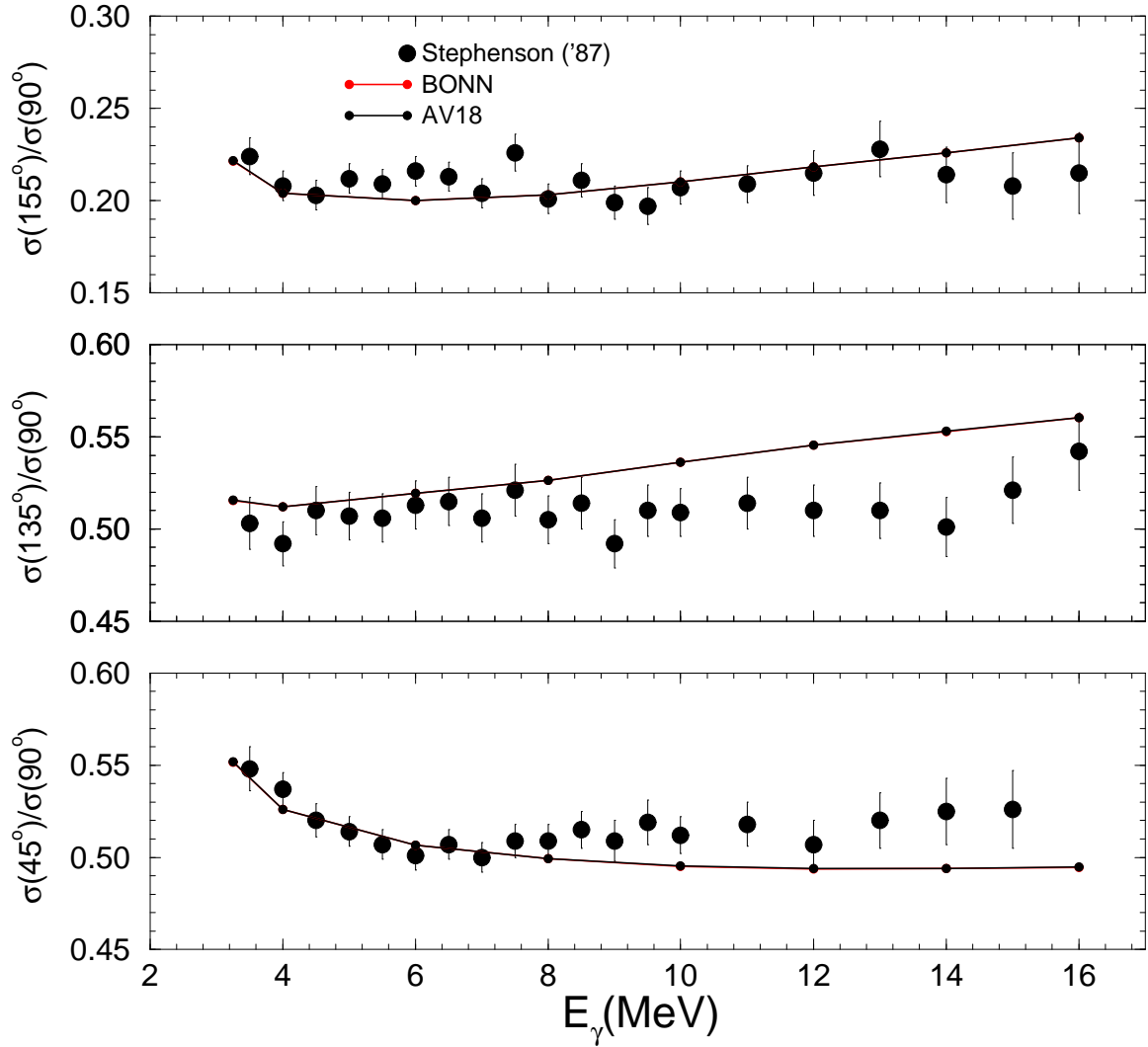


FIG. 3: (Color online) The lab-frame angular distribution ratios, measured in the deuteron photo-disintegration as function of photon energy, are compared to the results of calculations based on the BONN and AV18 potentials. Note that the theoretical curves are indistinguishable.

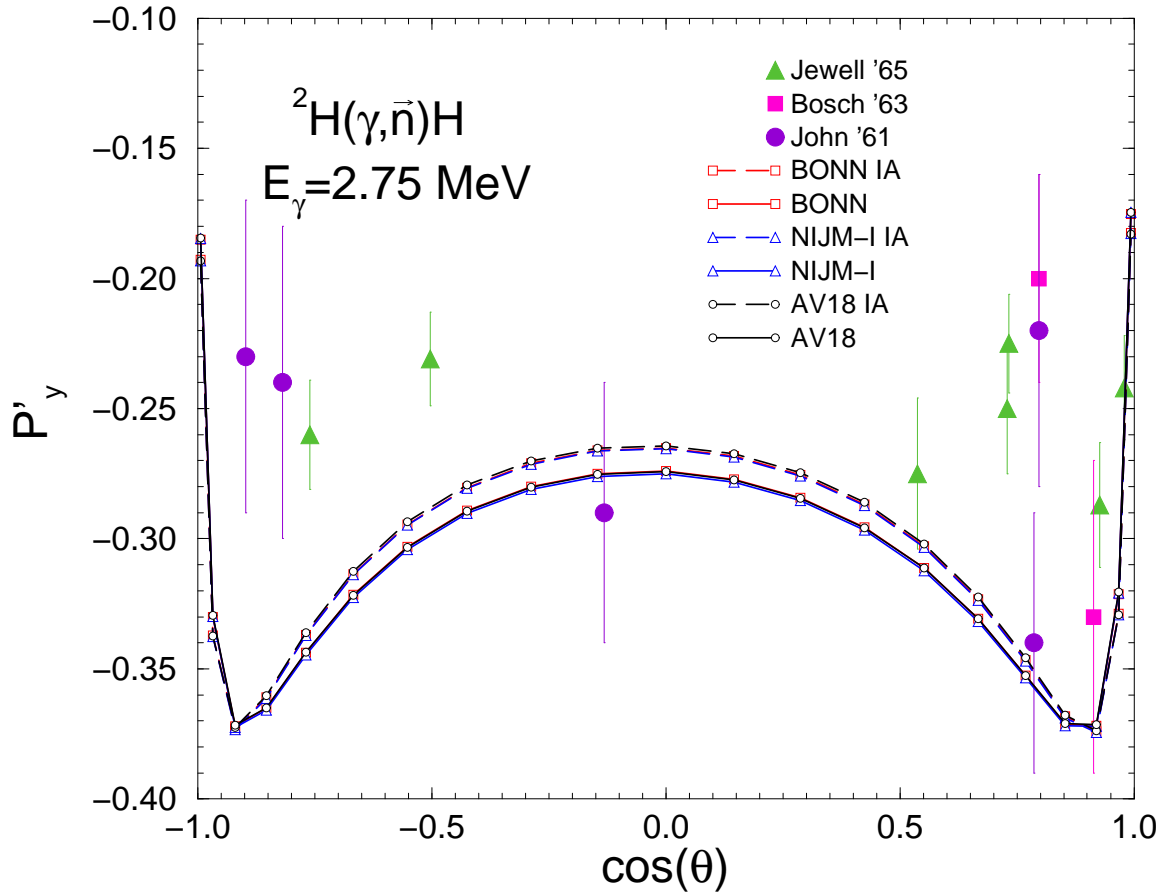


FIG. 4: (Color online) The center-of-mass angular distribution of the neutron induced polarization measured in the ${}^2\text{H}(\gamma, \vec{n}){}^1\text{H}$ reaction at photon energies of 2.75 MeV is compared to the results of calculations based on a number of latest-generation nucleon-nucleon potentials and a realistic model for the nuclear electromagnetic current, including one- and two-body components. Also shown are the results obtained by ignoring two-body currents (labeled IA).

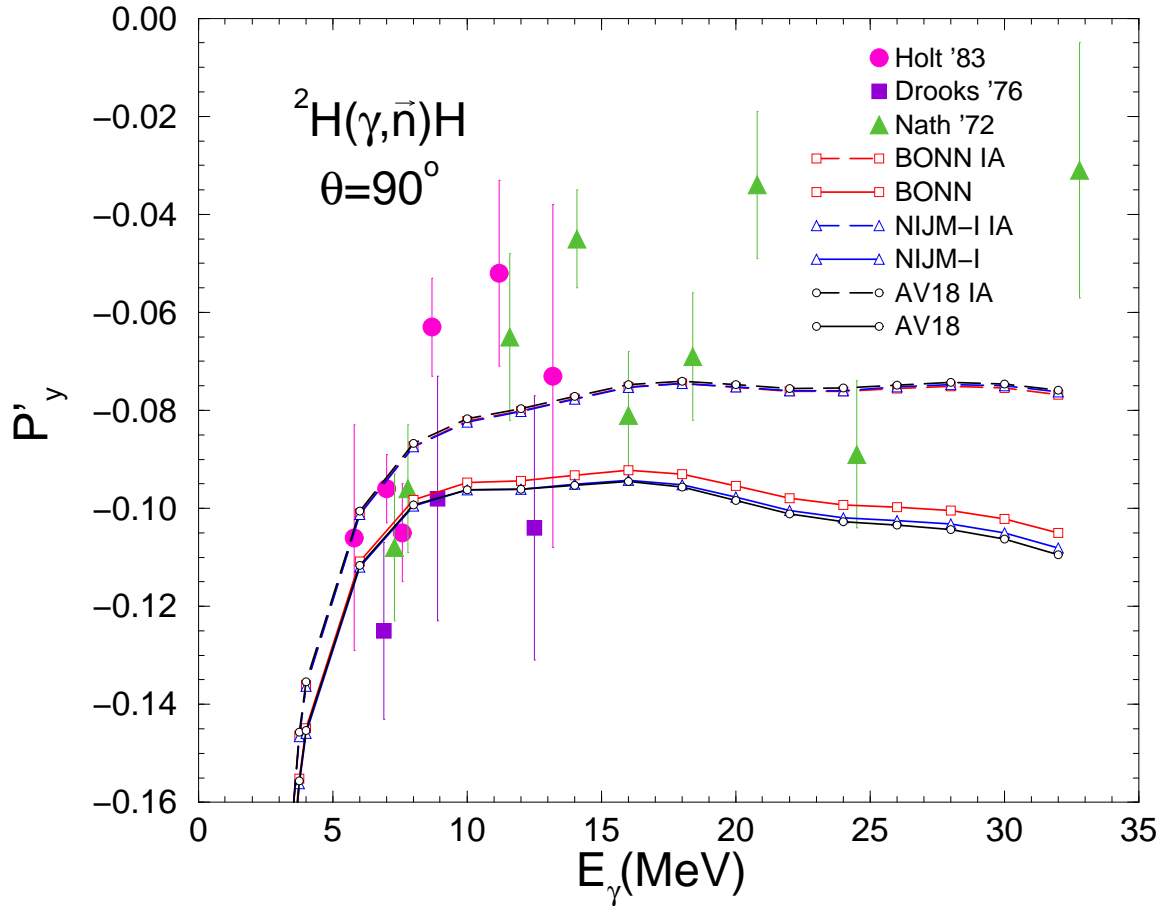


FIG. 5: (Color online) The neutron induced polarization measured in the ${}^2\text{H}(\gamma, \vec{n}){}^1\text{H}$ reaction at center-of-mass angle $\theta=90^\circ$ is compared to the results of calculations based on a number of latest-generation nucleon-nucleon potentials and a realistic model for the nuclear electromagnetic current, including one- and two-body components. Also shown are the results obtained by ignoring two-body currents (labeled IA).

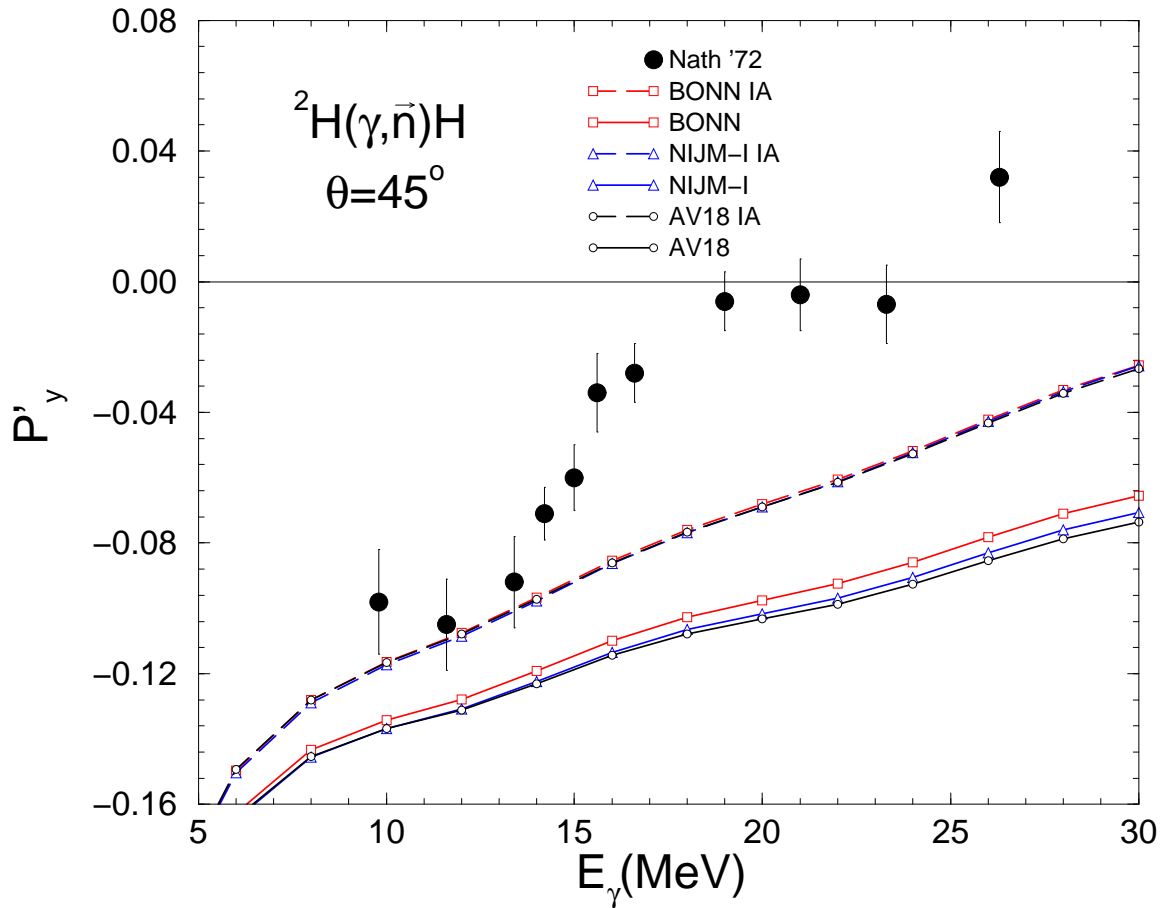


FIG. 6: (Color online) Same as in Fig. 5, but at center-of-mass angle $\theta=45^\circ$.

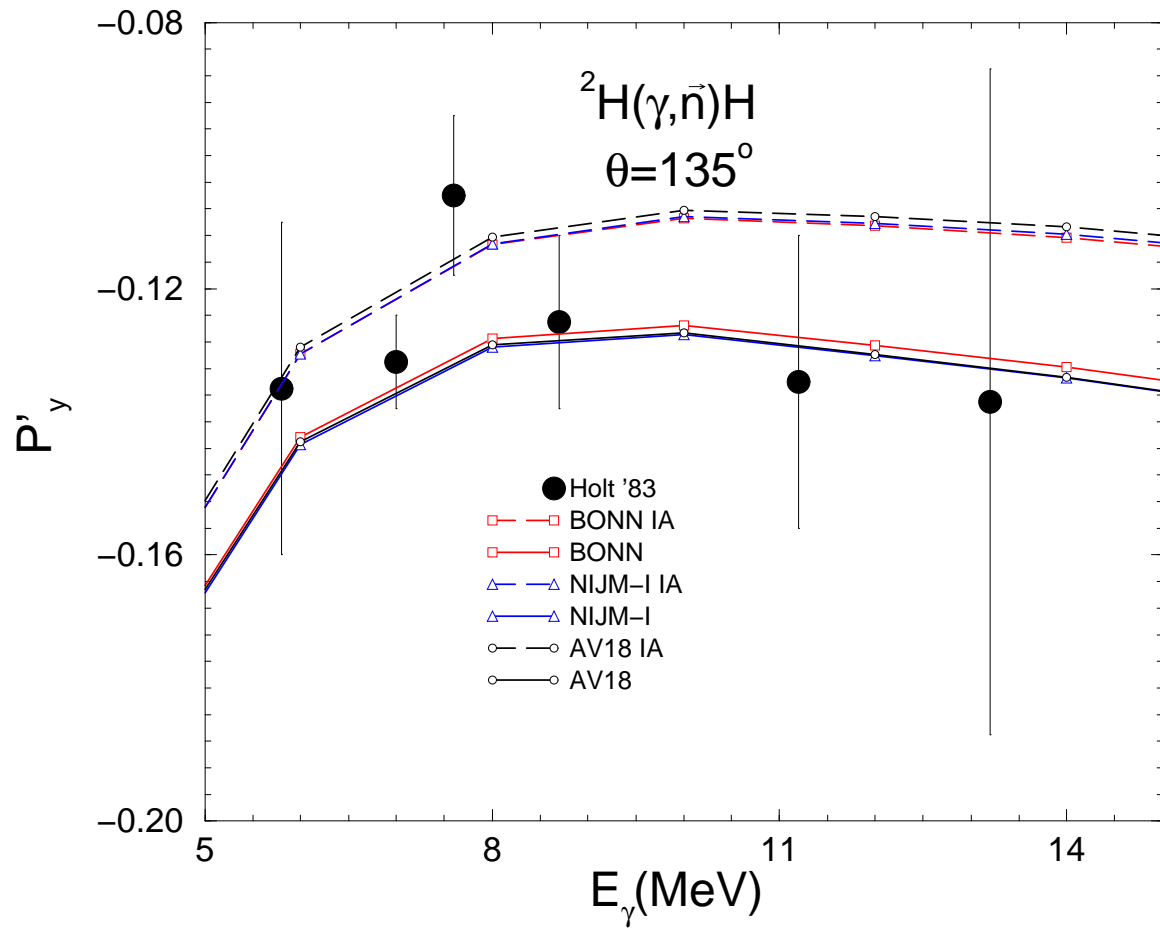


FIG. 7: (Color online) Same as in Fig. 5, but at center-of-mass angle $\theta=135^\circ$.

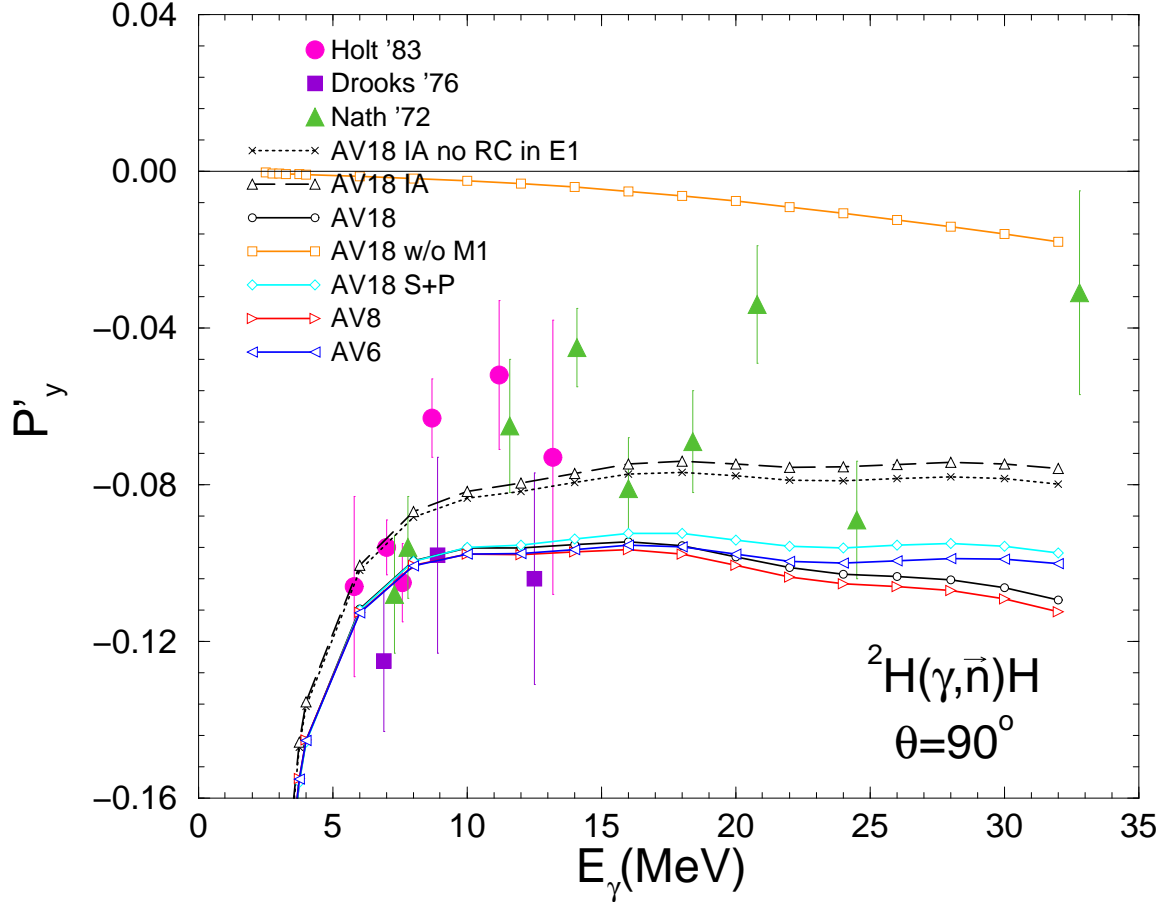


FIG. 8: (Color online) The neutron induced polarization measured in the ${}^2\text{H}(\gamma, \vec{n}){}^1\text{H}$ reaction at center-of-mass angle $\theta=90^\circ$ is compared to results obtained in various approximation schemes (see text for an explanation of the notation).